A new mechanism for the deployment of modular solar arrays: kinematic and static analysis

Stefano Seriani[1,3], Paolo Gallina[1], Lorenzo Scalera[2], Alessandro Gasparetto[2] and Armin Wedler[2]

[1] University of Trieste, Trieste, Italy
[2] University of Udine, Udine, Italy
[3] Robotik und Mechatronik Zentrum, Deutsches Zentrum für Luft- und Raumfahrt e.V. (DLR), Oberpfaffenhofen, Germany
gasparetto@uniud.it

Abstract. This paper presents a new solar arrays deployment mechanism for space applications. It consists of a modular kinematic structure, which is operated by a single cable (1 DoF). Compared to traditional methods, this mechanism has the advantage of being reversible in the movement. Kinematic analysis of the mechanism is carried out in this work, as well as static analysis. They allow to define the main actuation parameters such as cable pull tension and spring stiffness. Moreover, suitable values for the mechanism parameters are computed by means of a dedicated algorithm.

Keywords: solar arrays deployment, cable-based mechanisms, foldable mechanisms.

1 Introduction

In planetary explorations, the possibility of automating the deployment of solar arrays stored in transportable modules through robotic systems is of primary importance [1].

Space-faring systems have benefited from solar panel arrays since early in the exploration of space, the first notable example being Vanguard 1. Soon after, the first examples of deployable solar panels (Explorer 6 and Pioneer 5) demonstrated the advantages in terms of power output and small footprint [2]. In recent times, many systems have become available, especially for orbital systems. However, the large majority are non-reversible mechanisms, which means that the deployment operation cannot be undone [3-6]; reversible deployment systems [7-9] have been studied but seldom implemented in real missions since there is limited need for reconfiguration in orbit; it is however of paramount importance in mobile or modular planetary architectures. For example, the Exomars rover due to the planet Mars in the early 2020 is equipped with a 4-axis solar panel array [10]; this allows the rover to orient the panels to increase light incidence, thus enhancing power production. This approach, however, is complex as it involves a large number of actuators and has thus multiple points

of failures; we propose a lightweight mechanism which takes advantage of a single actuator, while at the same time providing deployment reversibility.

Since the top surface area of the module is comparably small ($\approx 0.1\ m^2$), and since power production is directly proportional to surface area, an efficient solar power deployment mechanism is essential. Four basic configurations are approachable:

i. Two-panel, storable array,
ii. Four-panel, foldable, storable array,
iii. Sun-tracking, foldable, storable array,
iv. Multi-panel, ground-deployed, foldable, storable array.

Conceptual illustrations are visible in Fig. 1, a), b), c) and d) respectively; in this paper, focus is set on the fourth configuration. If the area of the solar panels is taken into consideration, with a carrying capacity of the robot of approximately 20 kg, the values shown in Table 1 are obtained. A panel efficiency of 30% was considered [11], as well as a maximum solar irradiance of 1361 W/m^2 on the Moon [12] and around 300 W/m^2 on Mars [13], depending on the conditions of the atmosphere. The mass of the panels was estimated based on the data of NASA's Juno spacecraft [14]. Optimal, as well as average values are given, where the first refers to the sun at the zenith, while the former relates to a 45° solar incidence. The multi-panel configuration ensures the highest power production of the considered arrays, while at the same time being completely passive after deployment, contrary to, for example, the sun-tracking array. Furthermore, the stability of the module is not hindered by the panels, as is the case with the first two configurations.

Table 1. Achievable surface, mass and optimal power output of the four modules configurations.

			Power output [W]			
	Surface	Mass	Moon		Mars	
	[m^2]	[Kg]	Optimal	Average	Optimal	Average
i	0.25÷0.3	1.5	122	86	27	19
ii	0.5÷1.2	4.7÷8	490	346	108	76
iii	0.4÷0.6	>8	245	245	54	54
iv	1÷2.7	6÷12	1102	779	242	171

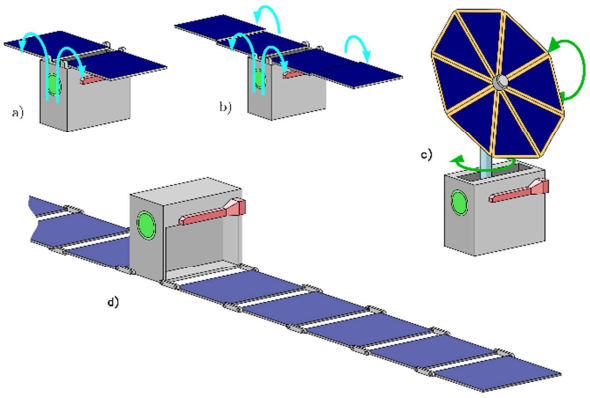

Fig. 1. Solar panel-equipped payload modules configurations.

As a mechanism, the multi-panel solar array shown in Fig. 2, is a planar serial chain which has a set of constraints on the rotations of each link (90°). This chain is loaded with a spring-based mechanism when folded – or stored – inside the module; during the unfolding and folding procedures a cable is used to actuate each link. The cable is wound around the entire array and this allows the complete "roll-up" to a stored configuration.

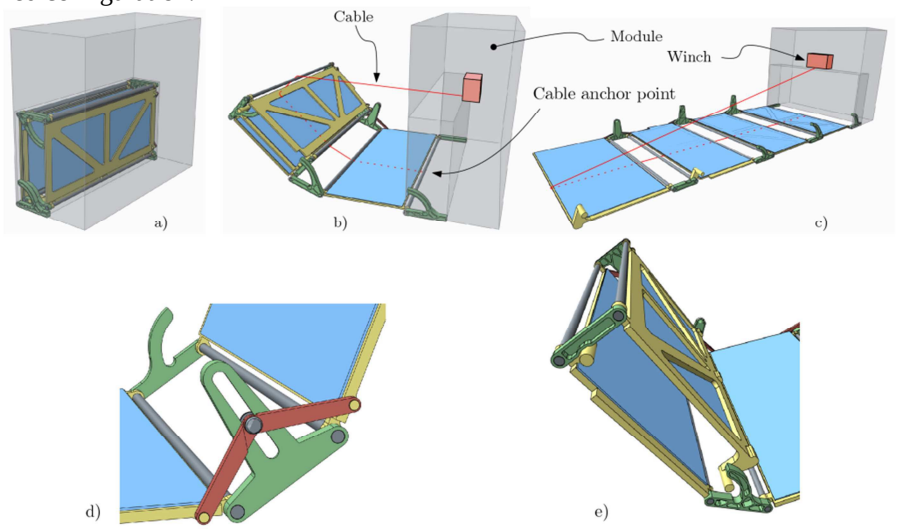

Fig. 2. A 3D model of the multi-panel, ground-deployed, foldable, storable solar array. The panels are shown in blue, while the structural links are in yellow. Green indicates the hinges assemblies. In a) the array is shown in its stored phase, inside the slot in the module. In b) the deployment of the second panel is shown, whereas in c) the fully deployed array is visible. In d) and e) the auxiliary mechanisms are shown, respectively the double quadrilateral and the lock guide.

Each section of the array is composed of a panel segment (in blue-yellow, in the Fig. 2), and a hinged segment (in green). The hinged segments are necessary in order to provide the necessary spacing between the panels, when in the stored position. These segments are deployed by means of the double quadrilateral mechanism highlighted in Fig. 2d.
In Fig. 2e, a set of curved guides is shown. The purpose of the guides is to constrain the folded panels in the stored position.

Each panel is connected to the next through a mechanical linkage composed of 6 revolution joints, a prismatic joint and a spring. A single cable actuates all the mechanisms. In literature, there are few examples of mechanical linkages operated by cables ([15-17]).
The paper is structured as follow: in Section 2, Kinematic and static analysis are performed. In particular, two conditions are introduced (the cable has to be always in tension and the system has to "remain folded" until it touches the ground during the deployment phase) to characterize the springs; in Section 3, a real case has been evaluated and discussed.

2 Kinematic and static analysis

There are three main aspects to consider in describing a model for the multi-panel solar array: the interaction between the cable and the segments of the serial chain; the double quadrilateral mechanism that provides the moments for the deployment through a spring-based action; the consequences of friction in the lock guides and the constraint that the guides provide.

Let us consider the deployment of a general section i of a solar panel array formed by n sections (see Fig. 2c). Equilibrium equation on the spring allows to calculate the force acting on point A_i:

$$\boldsymbol{F}_{link,i,1} = \frac{1}{2}\left(\frac{A_i - B_i}{\|A_i - B_i\|}\right)\left\|\boldsymbol{F}_{k,i}\right\| cos\,\beta_i \tag{1}$$

The same applies for $\boldsymbol{F}_{link,i,2}$, related to β_i. It follows easily that $\boldsymbol{M}_{Q,i} = (\boldsymbol{Q}_i - \boldsymbol{A}_i) \times \boldsymbol{F}_{link,i,1}$ and $\boldsymbol{M}_{P,i} = (\boldsymbol{A}'_i - \boldsymbol{P}_i) \times \boldsymbol{F}_{link,i,2}$. For sake of simplicity, the equilibrium of moments has been calculated in point $\boldsymbol{Q}_i$. Therefore, an *equivalent deployment moment* $\boldsymbol{M}_{depl,i} = \boldsymbol{M}_{P,i} + \boldsymbol{M}_{Q,i} = f(\vartheta_i)$ can be introduced, according to the principle of virtual works. The tension on the cable $\boldsymbol{F}_{depl,i}$ as a function of ϑ_i can be determined from the following equilibrium equation:

$$\boldsymbol{M}_{depl,i}(\vartheta_i) \cong \overline{\boldsymbol{Q}_\iota \boldsymbol{P}_{\iota+1}} \times \boldsymbol{F}_{depl,i} + \overline{\boldsymbol{Q}_\iota \boldsymbol{G}_\iota} \times m_i \boldsymbol{g} \tag{2}$$

where $m_i = \sum_{j=i}^{n} m_{p,j}$ is the sum of all the contributions of the folded panels; $m_{p,j}$ is the mass of the j^{th} panel and hinge. Applying the principle of virtual works, the error introduced by the previous equation is given by $\overline{\boldsymbol{Q}_\iota \boldsymbol{P}_\iota} \times \boldsymbol{F}_{depl,i}$, which is neglectable for small values of $\overline{\boldsymbol{Q}_\iota \boldsymbol{P}_\iota}$.

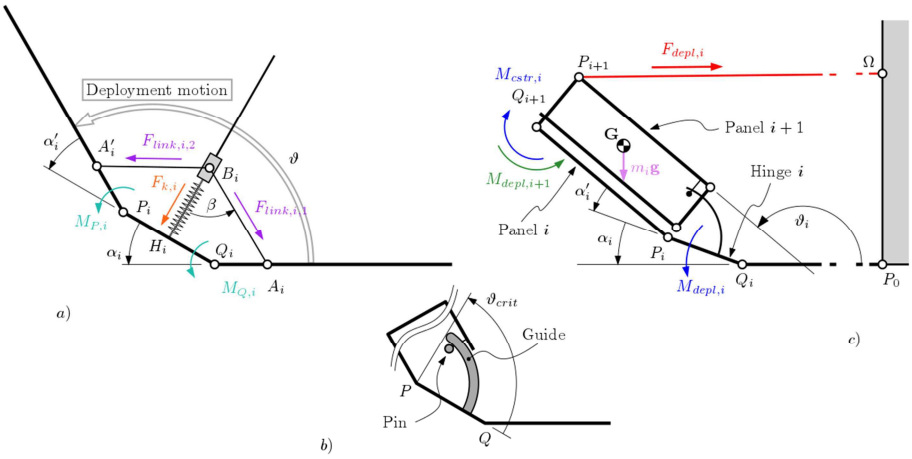

Fig. 3. General definition of the geometrical entities and values of the kinematic chain. In a) the geometrical and force entities are illustrated that constitute the hinged segments. The subscript indicates the section in the chain. In b) the constraint guide geometry is illustrated. In c) the global configuration of the panels is shown, along with the main parameters and forces.

In order for the mechanism to operate properly during the deployment phase, the module of the vector (cable tension) has to remain always positive (**Condition I**). Naming the unit vector of the reference frame (rightward direction), and assuming that the cable is almost horizontal, the condition becomes:

(3)

Let us define as the minimum value of torque ( ) capable to unfold the mechanism.

In general, the main condition that allows the mechanism to "remain folded" before touches the ground during the deployment is the following (**Condition II**):

(4)

where the first member is the sum of the moment generated by around and the contribution of the gravity force, and . The second member tends to unfold the mechanism.

In other words, during the deployment of the segment, the moment generated by the cable and by the gravitational force must be higher than the moment generated by the spring in the hinged segment.

The definition interval of the angle is limited by the angle and . The panels are constrained in a closed position by the guide on the bottom right of the sub-figure in the interval (see Fig. 3b).

Let us define as the minimum value of torque that satisfies Eq. (4). This value can be increased by a factor that works as a *factor of safety*.

The constraint guides that are responsible for are a source of friction as well. This can be modeled as,

$$\boldsymbol{M}_{\mu,i} \cong \mu r_{g,i}\left(\boldsymbol{M}_{depl,i+1}/\|\boldsymbol{Q}_{i+1} - \boldsymbol{P}_i\|\right) \tag{5}$$

where the factor in parentheses is the radial force caused by the spring mechanism in the $(i+1)^{th}$ hinge and $r_{g,i}$ is the radius of the i^{th} guide. In general it happens that $\boldsymbol{M}_{\mu,i} \ll \boldsymbol{M}_{depl,i}$, since $r_{g,i} \ll \|\boldsymbol{P}_{i+1} - \boldsymbol{Q}_{i+2}\|$, hence, for the purpose of this paper, we will disregard it.

It is possible, from these considerations, to define a backwards procedure to compute the moments and forces that ensure Eqn.s 3 and 4 are satisfied for each link in a chain with n elements:

i. Determine $\widetilde{\boldsymbol{M}}_{depl,n}$ by using Eq.s 1 (the moment generated by the spring system seen in Fig. 3c;
ii. Calculate the value of $\boldsymbol{F}_{depl,n}\ \forall\, \vartheta_n \in [\vartheta_{crit,n}, \pi]$ here called $\widetilde{\boldsymbol{F}}_{depl,n}$, from eq. 2 (the cable tension produced by the deployment moment $\widetilde{\boldsymbol{M}}_{depl,n}$), while verifying that eq. 3 is satisfied
iii. Calculate $\widetilde{\boldsymbol{M}}_{cstr,n-1}$ from $\widetilde{\boldsymbol{F}}_{depl,n}$ while verifying that the condition in Eq. 4 is satisfied (the minimum moment required to keep the next panel in the chain folded);

Steps i–iii can be iterated, for $n-1, n-2, \ldots, 0$ until $\widetilde{\boldsymbol{M}}_{depl,0}$ is reached. The input to this procedural computation is the value of the spring force of the n-th panel $\boldsymbol{F}_{link,n,1}$ and the masses m_i of the panels; the outputs are the deployment moments $\widetilde{\boldsymbol{M}}_{depl,i}$ of all the n panels. At this point, the procedure allows to derive a direct relation $\boldsymbol{M}_{depl,n-1} \longrightarrow \boldsymbol{M}_{depl,0}(n)$, starting from the inputs.

Once the $\boldsymbol{M}_{depl,i}$ values have been determined for every link , the springs can be fully characterized by means of Eq. (1). It should be noted that for this purpose the inequality in Eq. 4 defines the minimum load with the fully deployed section. As springs generally produce non-constant force over the elongation interval, both a maximum and minimum values can be separated.

Optionally, one could conceive the use of non-linear springs.

3 Discussion

Having defined a complete model for the multi-panel solar array and at the same time the algorithm for solving it, the main values for the mechanism presented in the previous Section are illustrated. In TABLE 2 the deployment moments $\widetilde{\boldsymbol{M}}_{depl,i}$ for each section i are reported, along with the maximum moments of $\widetilde{\boldsymbol{M}}_{\mu,i}$ generated by the friction on the constraint guides and the forces $\boldsymbol{F}_{depl,i}$ acting on the cable. In general, it seems that the deployment moment $\widetilde{\boldsymbol{M}}_{depl,i}$ applied to the zeroth hinge grows with n. It is immediately apparent that $\widetilde{\boldsymbol{M}}_{\mu,i} \ll \widetilde{\boldsymbol{M}}_{depl,i}$ in every occurrence; this is a strong evidence that the guide friction can be safely neglected during the computation, as expected. A friction coefficient of $\mu = 0.5$ was used.

TABLE 2. Deployment Torques Comparison. The values of and are shown for the 4 sections of the multi-panel solar array for gravity values relative to the surfaces of the Earth, Mars and the Moon.

.

Celestial body	**Interaction**	**Links ( )**			
		0	1	2	3
Earth	[Nm]	8.83	2.79	1.33	0.62
	[Nm]	0.08	0.03	0.01	–
	[N]	78.69	26.9	13.7	19.2
Mars	[Nm]	3.34	1.06	0.51	0.23
	[Nm]	0.03	0.01	<0.00	–
	[N]	29.78	10.18	5.18	7.27
Moon	[Nm]	1.46	0.46	0.22	0.1
	[Nm]	0.01	<0.00	<0.00	–
	[N]	13.01	4.45	2.27	3.18

The influence of the parameter is paramount; as our research shows, this parameter has a huge impact on the increment speed of along the links. Indeed, the exponential relation occurs.

Having defined the deployment moments for the links of the chain, the forces produced in the quadrilateral mechanism illustrated in Fig. 3a can be computed using Eq. 1. This shows comparably large values for the zero-th link; however, it should be noted that these values are strongly dependent on the geometry of the mechanism, with the overall value decreasing when the size of the involved entities (e.g. the links, or the distance) increases. In general, this means that the larger the mechanism, the lower the force needed; this ultimately calls for a trade-off, which should be carefully determined.

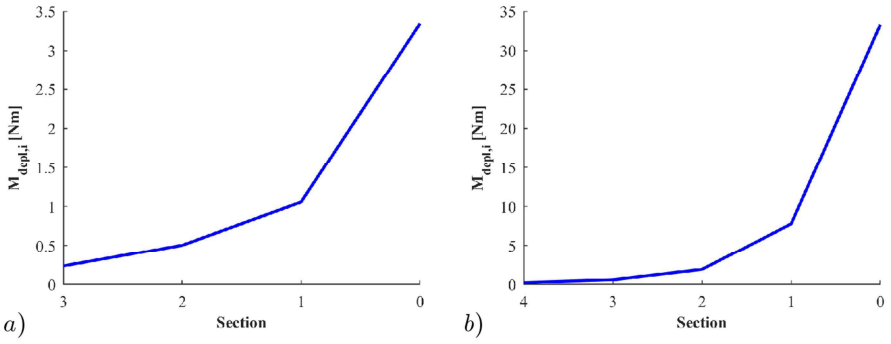

Fig. 4. Results of the algorithm on the surface of Mars ( ). In a), the figure shows , computed with . In b) a comparison of the algorithm is shown, with

.

8

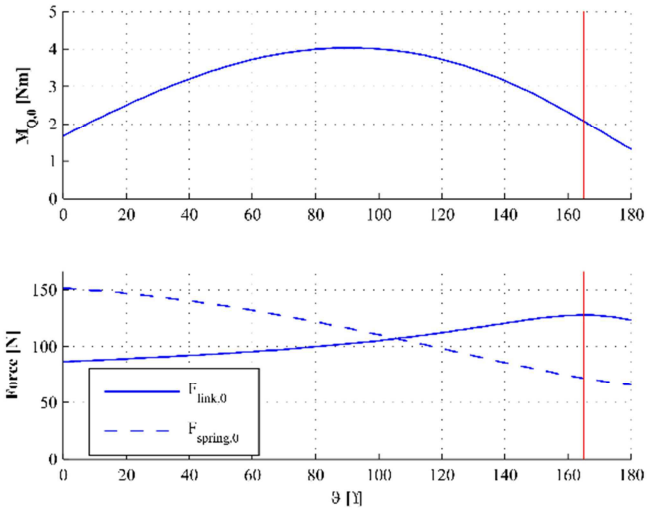

Fig. 5. Forces acting on the double quadrilateral mechanism of the 0^{th} link. In the top plot the values of the moment is shown, whereas in the bottom one those of the forces and , which act on the links (solid) and on the spring (dashed), are illustrated. The red line marks the location of .

The computation of a 5-links system is shown in Fig. 4 as an extension to the 4-links one. It should be noted that a slightly higher value was used. Indeed, with (Fig. 4, a), the 2^{nd} condition cannot be satisfied. In general, we find that values of give adequate results with this geometry.

With regards to the spring-loaded actuation of the links, the result of the double quadrilateral described are shown in Fig. 5 for the most loaded link, that is, the zero-th. By exploiting the model, Eq. 1, and thanks to some basic geometry, it is possible to compute the forces acting on the mechanism as a function of . In particular, starting with the (see TABLE 2, Mars scenario), it is possible to determine the spring characteristics and consequently the loads on the mechanism. In particular, we found a value of to be suitable. The forces illustrated in the bottom plot of the figure show values below 130 N on each link, peaking at 150 N on the spring.
A peculiarity of this mechanism is that is causes a beneficial excess of torque at as is visible in the figure.

4 Conclusion

A new solar arrays deployment mechanism for space applications has been conceptualized. It consists of a modular kinematics structure, which is operated by a single cable (1 DoF). This mechanism has the advantage of being reversible in the kinematic movement. The mechanism is made up of a series of panels connected by means of a linkage and a two symmetric springs. The paper presented an algorithm capable to

calculate the values of the parameters to be included in the deployment mechanism: the value of the spring stiffness that provides the stored energy to unfold the mechanism and the minimum value of the cable tension needed to fold the mechanism.

Acknowledgments

This work was supported in part by the Helmholtz Association, project alliance ROBEX, under contract number HA-304.

References

1. Wedler, A. et al.: First Results of the ROBEX Analogue Mission Campaign: Robotic Deployment of Seismic Networks for Future Lunar Missions, 68th International Astronautical Congress (IAC) (2017).
2. Flood, D.J.: Space photovoltaics - History, progress and promise, Modern Physics Letters B, 15, 561-570 (2001).
3. Lee, D.Y. et al.: Maximizing photovoltaic power generation of a space-dart configured satellite, Acta Astronautica, 111, art. no. 5335, 283-299 (2015).
4. Holland, A.F. ed al.: Consideration of the use of origami-style solar panels for use on a terrestrial/orbital wireless power generation and transmission spacecraft, Proceedings of SPIE - The International Society for Optical Engineering, 9865, art. no. 98650E (2016).
5. Zimmermann, C.G. et al.: Development of a New, High-Power Solar Array for Telecommunication Satellites, E3S Web of Conferences, 16, art. no. 01006 (2017).
6. Santoni, F.: Dynamics of spring-deployed solar panels for agile nanospacecraft, Journal of Aerospace Engineering, 28 (5), art. no. 04014122 (2015).
7. Kumar, P. and Pellegrino, S.: Deployment and retraction of a cable-driven rigid panel solar array, Journal of Spacecraft and Rockets, 33 (6), pp. 836-842 (1996).
8. Li, Y. et al.: Dynamic responses of space solar arrays considering joint clearance and structural flexibility, Advances in Mechanical Engineering, 8 (7), 1-11 (2016).
9. Li, Y. et al.: Planar rigid-flexible coupling spacecraft modeling and control considering solar array deployment and joint clearance, Acta Astronautica, 142, pp. 138-151 (2018).
10. Ferrando, E. et al.: Photovoltaic Assemblies for the Power Generation of the Exomars Missions, E3S Web of Conferences, 16, art. no. 04002 (2017).
11. Wanlass, M.: Recent progress in developing ultra-thin, monolithic gainp/gaas/lngaas tandem solar cells, SPRAT XX 9/25-9/27 (2007).
12. Kopp G., Lean J.: A new, lower value of total solar irradiance: Evidence and climate significance, Geophys. Res. Lett. 38 (2011).
13. Spiga, A., Forget, F.: Fast and accurate estimation of solar irradiance on Martian slopes, Geophysical Research Letters, 35 (15) (2008).
14. David, L.: Juno to Jupiter: Piercing the veil, Aerospace America, 49 (7), 40-45 (2011).
15. Seriani, S., Seriani, M., Gallina, P.: Workspace optimization for a planar cable-suspended direct-driven robot, Robotics and Computer-Integrated Manufacturing, 34, 1-7 (2015).
16. Pigani, L., Gallina, P.: Cable-direct-driven-robot (CDDR) with a 3-link passive serial support, Robotics and Computer-Integrated Manufacturing, 30 (3), 265-276 (2014).
17. Trevisani, A., Gallina, P., Williams II, R.L.: Cable-Direct-Driven Robot (CDDR) with passive SCARA support: Theory and simulation, Journal of Intelligent and Robotic Systems, 46 (1), 73-94 (2006).